Response of OH airglow emissions to the mesospheric gravity waves and its comparisons with full wave model simulation at a low latitude Indian station

R. N. Ghodpage[1], M. P. Hickey[2], A. Taori[3,4], Devendraa Siingh[5] and P. T. Patil[1]

[1] {Indian Institute of Geomagnetism, Shivaji University Campus, Kolhapur 416004, India}

[2] {Embry-Riddle Aeronautical University, FL - 32114, USA}

[3] {National Atmospheric Research Laboratory, Pakala Mandal, Gadanki (A. P.) 517112, India}

[4] {now at- National Remote Sensing Center (NRSC), Hyderabad, 500037, India}

[5] {Indian Institute of Tropical Meteorology, Pune-411 008, Maharashtra, India}

Abstract:

The quasi-monochromatic gravity wave induced oscillations, monitored using the mesospheric OH airglow emission over Kolhapur (16.8°N and 74.2°E), India during January to April 2010 and January to December 2011, have been characterized using the Krassovsky method. The nocturnal variability reveals prominent wave signatures with periods ranging from 5.2-10.8 hr as the dominant nocturnal wave with embedded short period waves having wave periods 1.5-4.4 hr. The results show that the magnitude of the Krassovsky parameter, viz., |η| ranged from 2.1 to 10.2 for principal or long nocturnal waves (5.2 to10.8 hr observed periods), and, from 1.5 to 5.4 for the short waves (1.5 to 4.4 hr observed periods) during the years of 2010 and 2011, respectively. The phase, i.e., Φ values of the Krassovsky parameters exhibited larger variability and varied from −8.1° to −167°. The deduced mean vertical wavelengths are found to be approximately −60.2 ± 20 km and – 42.8 ± 35 km for long and short wave periods for the year 2010. Similarly, for 2011 the mean vertical wavelengths are found to be approximately −77.6 ± 30 km and – 59.2 ± 30 km for long and short wave periods, respectively, indicating that the observations over Kolhapur were dominated by upward propagating waves. We use a full wave model to simulate the response of OH emission to the wave motion and compare the results with observed values.We discuss the observed wave characteristics and cause of the noted differences.

Keywords: OH emissions, Mesospheric gravity wave, Full wave model

1. Introduction

The airglow Hydroxyl emissions (OH) have been oftenly used for studying atmospheric temperature variation in the mesopause region since the pioneering work of Meinel (1950) and its usefulness to derive. the rotational temperature (Greet et al., 1998, Bittner et al., 2000). The collision frequency of OH with the neutral atmosphere in the neighborhood of 90 km of altitude should be in an order to $10^4\,s^{-1}$ and the life time of the excited Hydroxyl emission is around 3 to 10 msec. (Mies, 1974). This ensures that the excited OH molecules in the rotational energy levels are in a thermal equilibrium with the atmospheric ambient gases (Sivjee & Hamwey, 1987, Takahashi et al., 1998). Thus, it is normally assumed that the rotational state of OH band is in Maxwell-Boltzmann distribution. The radiated light intensity provides a direct measure of OH quantum state distribution in the mesopause, if one knows the Einstein coefficients governing the emission. Meriwether (1975) arrived at an expression for the P1(2) and P1 (5) rotational lines of OH (8-3) band by making use of the vibration-rotation transition probabilities of Mies (1974). Therefore using two lines from a single band we can estimate the rotational temperature by the given quation (Mies, 1974):

$$T_{n,m} = \frac{E_{v'}(J'_m) - E_{v'}(J'_n)}{k \ln\left[\frac{I_n}{I_m}\,\frac{A(J'_m, v' \to J''_{m+1}, v'')}{A(J'_n, v' \to J''_{n+1}, v'')}\,\frac{2J'_m+1}{2J'_n+1}\right]}$$

Where Tn,m is the rotational temperature calculated from two line intensities, I_n and I_m, from rotational levels J'_n , J'_m in the upper vibrational level ν', to J''_{n+1} , J''_{m+1} in the lower vibrational level ν''. $E_v(J)$ is the energy of the level (J, v). $A(J'_n, v' \rightarrow J''_{n+1}, v'')$ is the Einstein coefficient, for the transition from J'_n, v' to $J''m, v''$. The intensity ratio between P1 (2) and P1 (5) lines of the

OH(8,3) band were used to obtain rotational temperature using the transition probabilities as given by Mies (1974). Often the observed temporal variations in the mesospheric hydroxyl OH night airglow intensities and rotational temperatures are caused by propagating gravity waves from the lower to the upper atmosphere.

The interaction of these upward propagating waves with the ambient and other waves contribute to the dynamical variability, which in turn is reflected in observed airglow intensity and temperature perturbations (Hines, 1997). Krassovsky (1972) introduced a quantity 'η' to characterize the wave-induced perturbations. This parameter, termed as 'Krassovsky's parameter', is now defined as $\eta = |\eta| e^{-i\Phi}$, where $|\eta|$ indicates the ratio of the amplitude variation between the emission intensity and temperature perturbations normalized to their time averages and Φ is the phase difference between the intensity wave and its temperature counterpart (e.g., Walterscheid et al., 1987; Taylor et al., 1991). It should also be mentioned here that apart from the pure dynamical processes η can also be affected by various other unknown parameters, such as the variation of local oxygen photochemistry (Hickey et al., 1993) and height variation of the emission layer which affects emission rates and temperature directly (Liu and Swenson 2003; Vargas et al., 2007). Although this can complicate studies of Krassovsky's parameter, it offers an opportunity to study the above aspects at the same time. Overall, once the physics and chemistry of emissions are well understood, the η values would offer a good tool to study the perturbations caused in a parameter (temperature, brightness/intensity) by measuring one under the assumption that gravity wave induced perturbations are of adiabatic nature.

Utilizing the above, many investigators have carried out observational as well as theoretical studies on the identification and characterization of gravity wave and tidal signatures with wave periodicities ranging from few minutes to several hours (e.g., Walterscheid et al.,

1987; Hecht et al., 1987; Hickey 1988a, b; Taylor et al., 1991; Takahashi et al., 1992; Reisin and Scheer 1996; Taori and Taylor 2006; Guharay et al., 2008; Ghodpage et al., 2012, 2013). However, observational studies of the magnitude and phase of η over a range of wave periods for a given location and season are sparse. Some of the notable observations of η for the OH emission have been performed by Viereck and Deehr (1989) in the wave period range of ~ 1 - 20 hr and by Reisin and Scheer (1996) near to the semidiurnal tidal fluctuations.

In the present work, we utilize the mesospheric OH emission intensity and temperature data obtained during January - April 2010 and January - December 2011, when clear and moonless nights allowed observations to exceed 5 hours duration. We deduce the Krassovsky parameters as a function of observed wave period and also infer the vertical wavelengths for the observed mesospheric waves. Further, we compare our estimates with the earlier results reported by various investigators. We also employ a full-wave model to simulate the effects of wave motions on the OH airglow. This model has been used previously to compare observations and theory of airglow fluctuations (e.g., Hickey et al., 1998; Hickey and Yu 2005). Here, the model is used to estimate the values of the amplitudes and phases of Krassovsky's ratio which are compared to those derived from the observations, making the present study unique as such model comparison over India has not been done before.

2. Instrumentation and Observations

The mesospheric OH observations are made using the multispectral photometer from Kolhapur (16.8°N, 74.2°E) (Ghodpage et al., 2013, 2014). We analyze the data from January - April 2010 and January-December 2011 when clear sky conditions prevailed for several nights. For the year

2010, 13 nights out of 45 nights of observation clearly showed wavelike features, while in 2011, 29 from 60 nights of data exhibited wavelike variations.

2.1 The multispectral photometer

Regular observations of the night airglow emissions, OI 630.0 nm, OI 557.7nm and OH Meinel (731 nm and 740 nm) band have been carried out at the low latitude station Kolhapur. We have operated multispectral photometer pointing to the zenith over Kolhapur. The filters have a band width of 1 nm and their temperature is controlled by a temperature controller at 24 ^{0}C. The temperature coefficient of filter is 0.011 nm/ ^{0}C. At 24^{0}C the transmission efficiency of filters is 40 - 70 %.We kept the integration time for each filter 15 seconds which results in repetition time of 90 seconds with an accuracy of approximately ±0.5% for line intensity. The photometer has F/2 optics with ~10° full field of view. The stepper motor rotation and sensing of the initial position is performed by computer controlled software. As the detector, the EMI9658B photomultiplier tube is used. An amplifier (high gain trans-impedance) is used to convert and amplify the very weak photomultiplier output current (in the range of nA) into corresponding voltage form. In the absence of standard calibration source, we have used relative intensities (arbitrary units). In order to study the wave features present in the MLT region, we consider clear sky nights having more than 5 hours of continuous OH band data as mentioned in earlier reports (e.g., Taori et al., 2005).

2.2 Full Wave Model

The full-wave model is a linear, steady-state model that solves the linearized Navier-Stokes equations on a high resolution vertical grid to describe the vertical propagation of acoustic-

121 gravity waves in a windy background atmosphere including molecular viscosity and thermal
122 conduction, ion drag, Coriolis force and the eddy diffusion of heat and momentum in the
123 mesosphere. The model description, including equations, boundary conditions and method of
124 solution has been described elsewhere (Hickey et al., 1997; Walterscheid and Hickey 2001;
125 Schubert et al., 2003). The neutral perturbations are used as input to a linear, steady-state model
126 describing OH airglow fluctuations (Hickey and Yu 2005).

127 The model solves the equations on a high resolution vertical grid subject to boundary
128 conditions, and allows quite generally for the propagation in a height varying atmosphere (non-
129 isothermal mean state temperature and height varying mean winds and diffusion). The linearized
130 equations are numerically integrated from the lower to the upper boundary using the tri-diagonal
131 algorithm described by Bruce et al. (1958) and Lindzen and Kuo (1969). The lower boundary is
132 set well below the region of interest and a sponge layer is implemented to avoid effects of wave
133 reflection in the airglow response. In this study the lower boundary (the bottom of the lower
134 sponge layer) is placed at 250 km below z = 0 (i.e., -250 km). The wave forcing is through the
135 addition of heat in the energy equation. The heating is defined by a Gaussian profile with a full-
136 width-at-half-max of 0.125 km. It is centered at an altitude of 10 km. A Rayleigh-Newtonian
137 sponge layer in addition to natural absorption by viscosity and heat conduction prevents spurious
138 reflection from the upper boundary. At the upper boundary (here 300 km altitude) a radiation
139 condition is imposed using a dispersion equation that includes viscous and thermal dissipation
140 (Hickey and Cole 1987). The mean state is defined using the Mass Spectrometer Incoherent
141 Scatter (MSIS) model (Hedin 1991).

142 A set of linear perturbation equations for the minor species involved in the OH emission
143 chemistry is solved using the approach described in Hickey (1988). This assumes that these

144 minor species have the same velocity and temperature perturbations as the major gas (which are
145 deduced from the full-wave model). A vertical integration of the volume emission rates through
146 the vertical extent of the OH layer provides the brightness and brightness-weighted temperature
147 perturbations, from which Krassovsky's ratio is determined. The OH chemistry we use is the
148 same as that used previously (Hickey et al., 1997) and is for the OH (8-3) emission. We also
149 determine the vertical wavelength at the peak of the OH emission layer evaluated from the phase
150 variations of the temperature perturbations determined by the full-wave model.

151

152 **2.3 Space borne measurements**

153 The Sounding of the Atmosphere using Broadband Emission Radiometry (SABER), on-board
154 the Thermosphere Ionosphere Mesosphere Energetic and Dynamics (TIMED) satellite, is a high-
155 precision broadband radiometer which measures limb radiance (orbital inclination at 74°) of the
156 terrestrial atmosphere in 10 selected spectral bands ranging from 1.27 to 15 μm. In the present
157 study, we note larger values of $|\eta|$ occur during 2011 compared to 2010 for long/principal
158 waves, which indicates a larger intensity to temperature perturbation ratio over Kolhapur during
159 the passage of the waves during 2011. This could be due to the differences in either the
160 background atmosphere or the dynamical processes. To identify the differences in the OH
161 emission layer in year 2010 and 2011, we scrutinize the OH volume emission rate profile for
162 Kolhapur region obtained from SABER. The selected latitude–longitude grids are 10°N to 20°N
163 and 70°E to 90°E representing Kolhapur. The criteria for the selection of SABER data are such
164 that: (i) the SABER pass should be during typical observation times (excluding twilight time).

165

3. Results and Discussion

To identify the wave structures in the data, we utilize the perturbation amplitudes normalized to their time averaged values (hereafter referred to as mean values) in the intensity and temperature data to calculate the Krassovsky ratio. To illustrate this, we show a typical example corresponding to the data obtained on 26-27 January 2011 in Figure 1. We plot the intensity deviations from their mean values in figure 1(a), while, the temperature deviations from their mean values are plotted in figure 1(b). We note that night airglow intensity variations show a long-period wave with embedded short-period oscillatory features. On this night, the mean airglow intensity is found to be ~ 1.83 arbitrary units and the mean temperature data is ~ 195.75 K. To identify the nocturnal variability plotted together with data as solid red lines are the of best-fit cosine model (e.g., Taori et al., 2005) as follows.

$$Y = A\cos\left[\pi\frac{(X - Xc)}{T}\right] \quad (1)$$

where, A is the amplitude of the fitted wave of half-period T with phase Xc , and X is the time. The solid red lines in figure 1 show the results of the best-fit cosine model. We observed the presence of ~ 8.2 ± 1.1 hr and 8 ± 1.3 hr waves with relative amplitudes (normalized to their mean values and converted to corresponding % amplitude) ~ 3.6 %0 and 25.64%, in the nocturnal temperature and intensity variability, respectively. Given the uncertainties involved in the observations, we consider these to be the same waves. Further, we compute the |η| value for this wave to be 7.12 ± 1.2. To identify the shorter period features in the data we obtain residuals from the best-fit model values. The figure 1c and 1d panels show the nocturnal variability of the residual intensity and temperature respectively. The best-fit model reveals the presence of ~ 4.2 ± 0.2 and 3.0 ± 0.8 hr wave in the temperature and intensity residuals, respectively. Once again

188 we treat these as the same wave for the reason explained above. The best-fit analysis shows the
189 amplitudes of this wave to be ~ 1.019 % and 3.75% arbitrary units in the temperature and
190 intensity data, respectively. Hence, the |η| value for short period waves is estimated to be 3.68
191 ±0.9. In general we note that in worst case, the maximum error in |η| values are <25%. The phase
192 difference between the intensity and temperature waves is obtained with the help of best-fit
193 parameters which were also verified with a cross correlation analysis. The phase of the principal
194 waves (maxima) (period ~8.2 hr) was ~ 24.88 hr in the temperature data and 24.4 hr in the
195 intensity data, which results in the phase difference of ~ 0.48 hr, i.e., Φ values of −21.07±12°.
196 Similarly, for the shorter period (period ~ 4.2 hr) the Φ values are estimated to be −114.3±20°.
197 We can also estimate the vertical wavelength with the help of Krassovsky's parameter following
198 the approach elaborated by Tarasick & Hines (1990).

199 $$\lambda z = \frac{2\pi\gamma H}{(\gamma - 1)|\eta| \sin(\phi)} \quad (2)$$

200 where $\gamma = C_p / C_v = 1.4$ is the ratio of specific heats, and H = 6 km is the scale height. This
201 formula is valid for zenith observations and for plane waves. It is not valid for the evanescent
202 waves. Equation (2), negative vertical wavelength corresponds to downward phase propagation
203 (i.e., upward energy propagation), and that means that temperature oscillations precede the
204 intensity oscillations in phase (e.g., Takahashi, et al. 1990). Using the above relation we find that
205 vertical wavelength for the two cases discussed above are ~ −51.5± 15 and −39.3± 40 km for the
206 long period and the short period waves, respectively. Note that the long period wave estimates
207 may be biased when the data length is comparable to that of the wave period and therefore in our
208 study we have considered only those waves whose periods are substantially less than the length
209 of the available data.

The above analysis was carried out on nighttime events recorded during 2010 and 2011 when the prominent wave features were visible. During the 2010 period, the principal nocturnal waves in the data show the wave periods vary from 5.2 to 10.8 hr with corresponding temperature amplitudes ranging from 2 to 13.8 K. Similarly for 2011, wave periods vary between 5.2 and 8.4 hr with corresponding temperature amplitudes lying between 1.1 K and 15.7 K. However, the intensity amplitudes of the principal waves vary from 7.9% to 49.9 % and 5% to 90% for 2010 and 2011, respectively. We note that the estimated $|\eta|$ values were found to range from 2.1 - 10.5 for the principal wave. In the case of the short period waves, the periods ranged from 1.5 to 4.4 hr (for 2010) and 2.8 to 4.4 hr (for 2011) with corresponding temperature amplitudes ranging from 0.68 K to 12.2 K and 0.4 K to 14.2 K. The corresponding intensity amplitudes fall in range between ~ 1.54% to 46.8% and 1.32% to 46.8 for 2010 and 2011, respectively. The phase (Φ) values also exhibit large variability for long (short) period waves, range in between −27° and −167° (−27° and − 150°) for 2010 and −8.1° and −65.2° (− 39.1° and −122.6°) for 2011. For 2010 the deduced vertical wavelengths are found to vary from – 32.2 km to −140 km and −24 km to −88 km for the long and short period waves, respectively. Similarly, for 2011 the deduced vertical wavelengths are found to vary from − 40 km to −102 km, and −26 km to −92.4 km for the long and short period waves, respectively.

In Figure 2a we plot our results for $|\eta|$ (hereafter η) with pink half-filled squares indicating the estimates for the year 2010 and olive half-filled squares for the year 2011. We plot Φ in Figure 2b using the same symbols as used in Figure 2a. For a comparison, we also show the values of η and Φ of the results from other investigations are shown (Viereck and Deehr 1989; Takahashi et al., 1992; Oznovich et al., 1995, 1997; Drob 1996; Reisin and Scheer 1996; Taylor et al., 2001; Lopez-Gonzalez et al., 2005). Also shown in the figure are the model estimates of

Schubert et al. (1991), Tarasick and Shepherd (1992a, b), Walterscheid and Schubert (1995). We also plot observed η and Φ values against their observed period in figure (2a1 and 2b1). In general, we note that the parameter η increases with wave period. It is evident that the observed η and Φ values in our study show a large spread in their distribution as compared to the model values. A similar spread in the distribution of observed values of η (Figure 2a) from 1.03 to 7.85 has also been observed by other investigators (e.g., Takahashi et al., 1992). It may be noted that the values of η for the OH data in our study lie somewhere between the model estimates and the values observed by other investigators. Also noteworthy in this figure is that our η values are closer to the model values reported by Tarasick and Shepherd (1992a) for the waves with horizontal wavelength 500 km. The phase 'Φ' values, on the other hand show significantly larger deviations from this model for 2010, while for 2011 the match between measured and modeled phases appear to be better. We note that our measurements of Φ matches somewhat with those reported by Viereck and Deehr (1989), while large differences with other investigators can be easily noted. The variation of Φ values with respect to the wave periodicity, obtained in the 2010 year clearly shows that most of the time we observe values to be higher than those obtained by different models.

Of the importance is that Reisin & Scheer (2001) found η values of 3.47±0.07 corresponding to the wave periods between 1000s and 3h. Our observed values of η (arithmetic mean, 4.4± 1 for 2010 year and 5.7±1.7 for 2011 year) for OH measurements agree well with this report. In another study based on long-term observations with a spectral airglow temperature imager (SATI) from a mid-latitude station, Lopez-Gonzalez et al. (2005) reported a mean value of η of approximately ~ 8.6 for the OH measurements with a larger variability than our observations show. In another report, Guharay et al. (2008), found that for wave periods ranging from 6 hr to

13 hr, values of η in between 1.7 to 5.4, while the phase varied from −13^{o} to − 90°. Similarly, Aushev et al. (2008) presented amplitudes of the Krassovsky parameter for wave periods of 2.2 to 4.7 hr which in range from 2.4 to 3.6 while the phase values in between – 63^{o} to −121°. It is noteworthy that our derived values broadly agree with Guharay et al. (2008, 2009), Reisin and Scheer (2001, 2004) and Viereck and Deehr (1989) while they are somewhat different from the values reported by Lopez-Gonzalez et al. (2005) which may be due to the fact that their observations corresponded to higher latitude than ours. It also remains to be seen that when mesopause altitude itself changes from low to high latitudes how would that reflects in the Krassovsky parameters.

The results of (η and Φ) shown in Figure 2 emphasize that there are significant differences in the Krassovsky parameters derived from one study to another. This we suspect to be caused by the variations in the altitudinal profile of oxygen and its effect on the η through the complex OH chemistry (Walterscheid et al., 1994). Another possibility over low latitudes was discussed by Makhlouf et al. (1995) who suggested the quenching caused by the perturbed molecules during their transitions from several vibrational levels. Winds also affect the OH response to gravity waves and therefore they will also contribute to the spread of values seen between the various observation studies (e.g., Sonnemann G. and M. Grygalashvyly, 2003).

Note that our observations as well as models show the phase Φ for OH to be a negative value indicating upward propagating waves (see Tarasick and Shepherd,1992a, b). In general we note that our Φ values, although on some occasions are closer to Viereck and Deehr (1989) observations, show deviations from other investigators and are larger than the model values on most occasions. Differences in theory and observation may be due to the horizontal wavelength assumed in the model and or the Prandtl number (ratio of kinematic viscosity to thermal

diffusivity) assumed. The Prandtl number is important in theoretical calculations and modeling, especially when in terms of dissipating waves owing to molecular viscosity and thermal diffusivity while they propagate in the atmosphere (Hickey 1988). An error in the Prandtl number assumption will affect the derived wave parameters (λ_z, η etc.), which will successively mask the actual ones. In this regard, Makhlouf et al. (1995) studied the variations in the η values by modifying the model proposed by Hines and using a photochemical dynamical model; however, they were still unable to explain the appearance of the negative phases appropriately. Hines and Tarasick (1987) found a wide range of η variability, a result supported by our measurements. Further, Hines and Tarasick (1997) subsequently discussed the necessary correction for thin and thick layer approximations for the calculation of η from airglow emissions due to gravity waves interaction. They also pointed out that OH emission intensity, which affects the derived η values, does not depend on the oxygen profile and other minor species, which contradicts the theory of Walterscheid et al. (1994), Schubert et al. (1991). The calculated vertical wavelengths (VW) for all the nights of the observation are shown in Figure 2c as pink half filled squares indicating the estimates for the year 2010 and olive half filled squares for the year 2011. Large differences exist from one night to another. The VW has a large variability ranging from – 41 km to −102 km (2010) and – 36.2 km to −140 km (2011) for long period waves, and, – 26 to −92.4 and – 24 to −88 km for short period waves period of 2010 and 2011 years respectively. In 2010 (and 2011) years, the mean VW values for long and short period waves are calculated to be −60.2 ± 20 km (−77.2 ± 40 km) and –42.8 ± 15 km (–59.2 ± 30) respectively. Further, unlike the clear dependency on the wave period noted in the Krassovsky parameters (η and Φ) no clear trend is noted in the calculated VW. We also plot the values reported by Reisin and Scheer (1996) and Lopez-Gonzalez et al. (2005) for a comparison.

It is noteworthy that for all the days the VW for the long period wave are higher than the VW of short period waves. We also observed that VW values calculated for 2011 year are larger than 2010 year calculated values.We note that the values reported by Reisin and Scheer (1996) are approximately −30 km with about 40 km variability, which is a good agreement with our values. However, Lopez-Gonzalez et al. (2005) observed VW values to be approximately −10 km deduced from their OH observations, which do not agree with our values. Further, Ghodpage et al. (2012) analyzed the long-term nocturnal data of 2004-2007 and also observed that the VW lies between 28.6 and 163 km. Recently, Ghodpage et al. (2013) studied the simultaneous mesospheric gravity wave measurements in the OH emission from Gadanki and Kolhapur, inferring mean VWs varying from – 26 to – 60 km for the Kolhapur observations. Takahashi et al. (1990) reported vertical wavelengths varying from 20 to 80 km, which is in agreement with our values.

4. Comparison with the Full Wave Model Results

Wave simulations were performed using the Full Wave Model (FWM) for which the representative inputs were taken for the duration of observations reported in section 3. The observations were conducted over an approximate one month period spanning February 8th and March 13th, and accordingly we used the middle date of this observation period (February 25th) in the MSIS model to represent the undisturbed mean state. The latitude used was 16.8° N, and the local time was midnight. Because the speed and direction of wave propagation were not determined from the observations, several simulations were performed for each wave period in which the direction of propagation (eastward, northward and westward propagation) and the phase speed (50 m/s, 100 m/s and 150 m/s) were varied. Note that the mean winds (not shown) in

these simulations were derived from the Horizontal Wind Model (HWM) using the same input parameters as used for the MSIS model. The derived meridional winds (not shown) are far smaller than the zonal winds for the conditions considered here, and so while results for eastward and westward propagation differed quite markedly, those for northward and southward propagation did not. Hence we considered only a single direction (northward) for meridional propagation.

We also performed a tidal simulation using an equivalent gravity wave model (Lindzen 1970; Richmond 1975), as implemented in an earlier study (Walterscheid and Hickey 2001). The horizontal wavelength and Coriolis parameter are adjusted to give maximal correspondence with a given tidal mode. Here, we performed calculations for the terdiurnal (3,3), (3,4), (3,5) and (3,6) modes using parameters provided by Richmond (1975). The simplifications inherent in this approach are discussed by Walterscheid and Hickey (2001).

Comparisons between the full wave model results for η, Φ and λ_z and the values inferred from the observations are shown in figure 3a, 3b and 3c, respectively. In figure 3a we compare the observed values of η for 2010 and 2011. The observed values of η are represented as pink and olive lower half-filled squares for 2010 and 2011, respectively. In figure 3a we note that at few of the longer wave periods, the observed values of η are in good agreement with the full wave model results. For short period waves the values of η inferred from the observations appear to be bounded by the model values for waves with horizontal phase velocities are 50 and 100 m/s, respectively. For example, for 3.6 hr wave periods, the average of the values of η inferred from the observations is 3.7, while the full wave model values lie between about 0.5 (for the 100 m/s wave) and 7 (for the 50 m/s, eastward propagating wave). For the 8 hr wave periods, the

347 average of the values of η inferred from the observations is 5.7, which is bounded by the full
348 wave model estimates for waves having a horizontal phase velocity of 50 m/s and different
349 propagation directions.

350 Overall, we note that the comparison between the observed η values and the modeled
351 values can be explained by gravity waves whose horizontal phase velocities range from 50 m/s to
352 100 m/s. In this regard, an earlier investigation by Pragati Sikha et al. (2010) reported observed
353 gravity wave horizontal phase speeds (for periods 5 min to 17 min) varying between 10 m/s and
354 48 m/s. The propagation directions were reported to be preferentially towards the north. More
355 recently, Taori et al. (2013) studied mesospheric gravity wave activity in the OH and OI 558 nm
356 emissions from Gadanki. They observed that the gravity waves were moving in the north–west
357 direction. The average phase velocity of the ripple-type waves was found to be 23.5 m/s. The
358 other, band-type waves, with horizontal scales of about 40 km, were found to be propagating
359 from south to north with an estimated phase speed of 90 m/s.

360 The vertical wavelengths (λ_z) calculated using the observed values of η and Φ differ
361 significantly from the full wave model estimate for waves with phase velocities below 100 m/s.
362 More typically, a comparison between those values inferred from the observations and those
363 derived from the model tend to agree for phase velocities in the 100 - 150 m/s range. However, it
364 should be noted that vertical wavelengths inferred from the observations are based on the use of
365 the inferred Krassovsky's ratio, η, in Eq. (2). Please note that the errors in the determination of
366 the phase (Φ) of η may lead to significant errors (proportional to cotΦ) in the determination of
367 λ_z, especially as Φ approaches $\pm 180^o$.

368 The differences noted in the observed and modeled estimates of Krassovsky ratio
369 magnitudes η and phase (Φ) may be associated with the limitation arising due to dynamics as

well as the measurements. In terms of measurements limitation, the parameters achieved with the best fit method may have leaked contribution from other wave components which may be dynamically varying within a wave period. In terms of dynamics, that full wave model uses climatological density (both major gas and minor airglow-related species) and wind profiles which will introduce uncertainties. This point has been previously elaborated by Walterscheid et al. (1994) with respect to the effect of a change in the [O] profile on the OH response to wave motions.

It is interesting to note that the arithmetic mean values of $|\eta|$ for the years 2010 and 2011 were 4.4 and 5.7 respectively. When we look at each $|\eta|$ value from one wave period range to other, the difference is found to be more than 30% which is well above the maximum errors in the estimation. One may further argue that this difference may not be significant. For this, we looked at the mode of the values for periods ranges 1-4 hr, 4-6 hr, 6-8 hr and 8-10 hr. We found that in each case in the year 2011 mode values are larger than the year 2010. The differences noted in the magnitude of the observed Krassovsky ratio η between 2010 and 2011 may be associated with variations in the height and shape of the undisturbed OH emission profile. We use the SABER data to investigate this aspect. To check whether there was a difference in the OH emission layer structure, we selected the nighttime OH emission profile for a grid encompassing 10^{o}N to 20^{o}N latitudes and 70^{o}E to 90^{o}E latitudes during February, March and April months of the years 2010 and 2011. We have selected the February to March period because the optical airglow data used in this study was acquired primarily during these months. The monthly mean values of OH emission rates are plotted in Figure 4. The solid curves correspond to 2010 data while the dashed curves correspond to 2011 data. We note that the peaks of OH emission layer during February, March and April of 2010 occurred at 84.2 km, 82.8 km

and 85.1 km altitude, respectively, while the corresponding peaks for 2011 were found to occur at 85.8 km, 85.6 km and 85.2 km altitude. This suggests that the peak of the emission layer occurred at a somewhat lower altitude in 2010 compared to 2011. Also, the mission rates during February and March were found to be higher in 2010. It is important to note that in an earlier study, Ghodpage et al. (2013) compared the Krassovsky ratios at two different latitudes, Gadanki (13.5 N, 79.2E) and Kolhapur (16.8°N and 74.2°E) and noted a lower OH emission layer peak over Kolhapur and also larger estimated η values over Kolhapur. In the present case, instead of the location, it is the difference in the measurement year where the peak emission altitudes of the OH emission layer are somewhat diffterent. As the peak emission layer arise due to the chemical reactions involving odd oxygen, it is proposed that chemical composition was different from the year 2010 to the year 2011. Therefore, the noted emission rates may be responsible for the observed differences in the Krassovsky parameters. A further question that arise here is why the peaks should be different from one year to the other. As these months are pre-monsoon, when a large scale oscillation namely,El Niño/Southern Oscillation (ENSO) sweeps through the south Asian continent, we looked at the ENSO strength based on the Multivariate ENSO Index (MEI). This index is shown in table 1, where it is noteworthy that the MEI index for 2010 (January to May) is of opposite sign to that for the corresponding months in 2011. We postulate that these large scale processes have a profound impact on the observed wave energetics and dynamics at mesospheric altitudes. Large scale processes induced the wave oscillations associated with the ENSO. The ENSO generates a spectrum of waves which are of planetary scales. These are expected to generate a secular variation in temperature and density structure throughout the atmosphere. A difference in ENSO suggests that these forcing are different in the two years (2010, 2011). At present, we do not know through which process the ENSO may have

implications in the observed wave characteristics. However, we believe that further investigation is required in order to confirm whether or not any such associations really do exist.

5. Conclusion:

We report the Krassovsky parameters for the observed gravity waves from Kolhapur (16.8°N and 74.2°E) and their comparison with the full wave model.

1) It is evident that the observed values of Krassovsky parameters in our study show a large spread in their distribution as compared to the model values (shown in Figure 2a). A similar spread in the distribution has also been reported by other investigators. We have also observed magnitude of η values is larger in the year 2011 than 2010.
2) It is also notable that the values of η for the OH data in our study lie between the model estimates and the values observed by other investigators. Whereas the phase values are more than the model values on most occasions. We note that our Φ measurements match with those reported by Viereck and Deehr (1989), while they show large differences with other investigators values.
3) Observed vertical wavelength (VW) values broadly agree with the range reported by other investigators and are found to vary from −26 to −140 km.We also noted that VW values calculated for 2011 year are larger than 2010 year calculated values. Most of wave propagating upward in direction.
4) Comparison of observed η and Φ values agree fairly well with the full wave model results for waves with 50 and 100 m/s horizontal phase velocities. Vertical wavelengths tend to agree for waves with 100 and 150 m/s horizontal phase velocities, except for the

longest period waves for which vertical wavelength cannot be reliably inferred from the observations.

The database used in the present study is limited in terms of the length and locations. Based on the above conclusions we emphasis that more rigorous study using coordinated observations and modeling are required to uncover the physics occurring at upper mesosphere.

Acknowledgements

This work is carried out under the research grant funded by Ministry of Science and Technology and Department of Space, Govt. of India. RNG thank the Director, Indian Institute of Geomagnetism (IIG), Navi Mumbai for encouragement to carry out this work. The night airglow observations at Kolhapur were carried out under the scientific collaboration program (MoU) between IIG, Navi Mumbai and Shivaji University, Kolhapur. MPH acknowledges the support of NSF grant AGS-1001074.

6. References

Aushev, V. M., Lyahov, V. V., Lopez-Gonzalez, M. J., Shepherd, M. G., and Dryna, E. A. :Solar eclipse of the 29 March 2006: results of the optical measurements by MORTI over Almaty (43.03°N, 76.58°E), J. Atmos. Sol. Terr. Phys., 70, 1088–1101, 2008.

Bruce, G. H., Peaceman, D. W., Rachford, Jr. H. H., and Rice, J. D.: Calculations of unsteady-state gas flow through porous media, Petrol. Trans. AIME, 198, 79-92, 1953.

459 Bittner, M., Offermann, D., Graeft.: Mesopause temperature variability above a midlatitude
460 station in Europe. Journal of Geophysical Research, 105(D2): 2045–2058, 2000.

461 Drob, D. P.: Ground-based optical detection of atmospheric waves in the upper mesosphere and
462 lower thermosphere, Ph. D. Thesis, University of Michigan, Ann Arbor, MI., 1996.

463 Ghodpage, R. N., Singh, D., Singh, R. P., Mukherjee, G. K., Vohat, P., and Singh, A. K.: Tidal
464 and gravity waves study from the airglow measurements at Kolhapur (India), J. Earth Syst.
465 Sci.121, 6, 1511–1525, 2012.

466 Ghodpage, R. N., Taori, A., Patil, P. T., and Gurubaran, S.: Simultaneous mesospheric gravity
467 wave measurements in OH night airglow emission from Gadanki and Kolhapur – Indian low
468 latitudes, Currents Science, 104, 1, 98-105, 2013.

469 Ghodpage, R.N., Taori, A., Patil, P. T., Gurubaran, S., Sharma, A. K., Nikte, S., and Nade, D.:
470 Airglow Measurements of Gravity Wave Propagation and Damping over Kolhapur (16.8^{o} N,
471 74.2^{o} E), International Journal of Geophysics (IJG), Volume 2014,1-9,
472 http://dx.doi.org/10.1155/2014/514937, 2014.

473 Greet, P.A., French, WJR., Burns, G B., Williams, PFB., Lowe, R. P., & Finlayson, K. :OH (6-2)
474 spectra and rotational temperature measurements at Davis, Antarctica, Annales Geophysicae,
475 16(1), 77–89, 1998.

476 Guharay, A., Taori, A., Bhattacharjee, B., Pant, P., Pande, P., and Pandey, K.: First ground-
477 based mesospheric measurements from central Himalayas, Current Science, 97, 664-669,
478 2009.

479 Guharay, A., Taori, A., and Taylor, M.: Summer-time nocturnal wave characteristics in
480 mesospheric OH and O_2 airglow emissions, Earth Planets Space, 60, 973–979, 2008.

481 Hecht, J. H., et all.: Observations of wave-driven fluctuations of OH nightglow emission bfrom
482 Sondre Stromfjord, Greenland, J. Geophys. Res., 92, 6091-6099, 1987.

483 Hedin, A. E. :Extension of the MSIS thermosphere model into the middle and lower atmosphere,
484 J. Geophys. Res., 96, 1159 – 1172, 1991.

485 Hickey, M. P., and Yu, Y.: A full-wave investigation of the use of a "cancellation factor" in
486 gravity wave-OH airglow interaction studies, J. Geophys. Res., 110, A01301,
487 doi:10.1029/2003JA01372, 2005.

488 Hickey, M. P., Huang, T.-Y., and Walterscheid, R.: Gravity wave packet effects on chemical
489 exothermic heating in the mesopause region, J. Geophys. Res., 108(A12), 1448,
490 doi:10.1029/2002JA009363, 2003.

491 Hickey, M. P., Walterscheid R. L., and Schubert, G.: Gravity wave heating and cooling in
492 Jupiter's thermosphere, Icarus, 148, 266-281, 2000.

493 Hickey, M. P., Walterscheid, R. L., Taylor, M. J., Ward, W., Schubert, G., Zhou, Q., Garcia, F.,
494 Kelley, M. C., and Shepherd G. G.: Numerical simulations of gravity waves imaged over
495 Arecibo during the 10-day January 1993 campaign, J. Geophys. Res., 102, 11,475-11,489,
496 1997.

497 Hickey, M.P., Schubert, G., and Walterscheid, R. L.: Gravity wave-driven fluctuations in the O_2
498 atmospheric (0-1) nightglow from an extended, dissipative emission region, J. Geophys.
499 Res., 98(13),717-730, 1993.

500 Hickey, M. P.: Effects of eddy viscosity and thermal conduction and coriolis force in the
501 dynamics of gravity wave driven fluctuations in the OH nightglow, J. Geophys. Res., 93,
502 4077, 1988.

503 Hickey, M.P., Taylor, M.J., Gardner, C.S., and Gibbons, C.R. Full-wave modeling of small-
504 scale gravity waves using Airborne Lidar and Observations of the Hawaiian Airglow
505 (ALOHA-93) O(1S) images and coincident Na wind/ temperature lidar measurements, J.
506 Geophys. Res. 103, 6439-6453,1998.

507 Hickey, M. P., and Cole, K. D.: A quartic dispersion equation for internal gravity waves in the
508 thermosphere, J. Atmos. Terr. Phys., 49, 889-899, 1987.

509 Hines, C. O.: A fundamental theorem of airglow fluctuations induced by gravity waves, J.
510 Atmos. Sol. Terr. Phys.,59, 319–326, 1997.

511 Hines, C. O., and Tarasick, D. W.: Layer truncation and the Eulerian/ Lagrangian duality in the
512 theory of airglow fluctuations induced by gravity waves, J. Atmos. Sol. Terr. Phys., 59, 327–
513 334, 1997.

514 Hines, C. O., and Tarasick, D. W. : On the detection and utilization of gravity waves in airglow
515 studies, Planet Space Sci., 35, 851–866, 1987.

516 Krassovsky, V. I.: Infrasonic variation of OH emission in the upper atmosphere, Ann. Geophys.,
517 28, 739–746, 1972.

518 Lindzen, R. S.: Internal gravity waves in atmospheres with realistic dissipation and temperature,
519 part I: Mathematical development and propagation of waves into the thermosphere, Geophys.
520 Fluid Dyn., 1, 303-355, 1970.

521 Lindzen, R. S., and Kuo, H. L.: A reliable method for the numerical integration of a large class
522 of ordinary and partial differential equations, Mon. Wea. Rev., 97, 732-734, 1969.

523 Liu, A. Z., and Swenson, G. R.: A modeling study of O_2 and OH airglow perturbations induced
524 by atmospheric gravity waves, J. Geophys. Res, 108, D4, 4151, doi:10.1029/2002JD002474,
525 2003.

526 Lopez-Gonzalez, M. J., et al.: Tidal variations of O_2 Atmospheric and OH(6-2) airglow and
527 temperature at mid-latitude from SATI observations, Ann. Geophys., 23, 3579–3590, 2005.

528 Makhlouf, U. B., Picard, R. H., and Winick, J. R.: Photochemical-dynamical modeling of the
529 measured response of airglow to gravity waves, 1: basic model for OH airglow, J. Geophys.
530 Res., 100, 11,289–11,311, 1995.

531 Mies, F. H.:Calculated vibrational transitions probabilities of OH ($X^2\pi$). Journal of Molecular
532 Spectroscopy, 53, 150–188, 1974.

533 Meinel, A. B.:OH Emission bands in the spectrum of the night sky I. Astrophys. J., 111, 555 –
534 564, 1950.

535 Meriwether, J. W.: High latitude airglow observations of correlated short term fluctuations in the
536 hydroxyl Meinel 8-3 band intensity and rotational temperature, Planet. Space Sci., 23, 1211–
537 1221, 1975.

538 Oznovich, I., Walterscheid, R. L., Sivjee, G. G., and McEwen, D. J.: On Krassovsky's ratio for
539 ter-diurnal hydroxyl oscillations in the winter polar mesopause, Planet Space Sci.,45(3), 385–
540 394, 1997.

Oznovich, I., McEwen, D. J., and Sivjee, G. G.: Temperature and airglow brightness oscillations in the polar mesosphere and lower thermosphere, Planet Space Sci., 43, 1121–1130, 1995.

Pragati, R.S., Parihar, N., Ghodpage, R., Mukherjee, G.K.: Characteristics of gravity waves in the upper mesosphere region observed by OH airglow imaging, Current Science 98, 392–397,2010.

Reisin, E.R., and Scheer, J.: Vertical propagation of gravity waves determined from zenith observations of airglow, Adv. Space Res. 27(10), 1743-1748, 2001.

Reisin, E. R., and Scheer, J.: Characteristics of atmospheric waves in the tidal period range derived from zenith observations of O_2(0-1) Atmospheric and OH (6-2) airglow at lower mid latitudes, J. Geophys. Res., 101, 21,223–21,232, 1996.

Richmond, A. D.: Energy relations of atmospheric tides and their significance to approximate methods of solution for tides with dissipative forces, J. Atmos. Sci., 32, 980-987, 1975.

Schubert, G., Hickey, M. P., and Walterscheid, R. L.: Heating of Jupiter's thermosphere by the dissipation of upward propagating acoustic waves, Icarus, 163, 398-413, 2003.

Schubert, G., Walterscheid, R. L., and. Hickey, M. P.: Gravity wave-driven fluctuations in OH nightglow from an extended, dissipative emission region, J. Geophys. Res., 96 (A8), 13,869–13,880, 1991.

Sivjee, G. G., & Hamwey, R. M.: Temperature and chemistry of the polar mesopause OH. Journal of Geophysical Research, 92(A5): 4663–4672, 1987.

Stubbs, L. C., Boyd, J. S., and Bond, F. R.: Measurement of the OH rotational temperature at Mawson, East Antarctica, Planet. Space Sci., 31 (8), 923–932, 1983.

562 Sonnemann G. and Grygalashvyly, M.: The zonal wind effect on the photochemistry within the
563 mesosphere / menopause region, Adv. Space Res. Vol. 32 (5), 719-724, 2003.

564 Takahashi, H., Buriti, R. A., Gobbi, D., and Batista, P. P.: Equatorial planetary wave signatures
565 observed in mesospheric airglow emissions, J. Atmos. Sol. Terr. Phys., 64, 1263–1272, 2002.

566 Takahashi, H., Sahai, Y., Batista, P. P., and Clemesha, B. R.: Atmospheric gravity wave effect
567 on the airglow O2(0-1) and OH (9-4) band intensity and temperature variations observed from
568 a low latitude station, Adv. Space Res.,12(10), 131–134, 1992.

569 Takahashi, H., Sahai, Y., and Teixeira, N.R.: Airglow intensity and temperature response to
570 atmospheric wave propagation in the mesopause region, Adv. Space Res. 10, (10)77-(10)81,
571 1990.

572 Takahashi, H, Batista, P. P, Buriti, R. A, Gobbi, D, Nakamura, T, Tsunda, T & Fukao S.
573 Simultaneous measurements of airglow OH emission and meteor wind by a scanning photometer
574 and the MU radar. Journal of Atmospheric and Solar-Terrestrial Physics, 60(17): 1649–1668,
575 1998.

576 Tarasick, D. W. and Hines, C. O.: The observable effects of gravity waves in airglow emission,
577 Planet. Space Sci., 38, 1105–1119, 1990.

578 Taylor, M. J., Gardner, L. C., and Pendleton, Jr. W. R.: Long-period wave signatures in
579 mesospheric OH Meinel (6,2) band intensity and rotational temperature at mid-latitudes, Adv.
580 Space Res., 27(6–7), 1171– 1179, 2001.

581 Taylor, M. J., Turnbull, D. N., and Lowe, R. P.: Coincident imaging and spectrometric
582 observations of zenith OH nightglow structure, Geophys. Res. Lett., 18, 1349–1352, 1991.

583 Taori, A., and Taylor, M. J.: Characteristics of wave induced oscillations in mesospheric O2
584 emission intensity and temperatures, Geophys. Res. Lett., 33, L01813,
585 doi:10.1029/2005GL024442, 2006.

586 Taori, A., Taylor, M. J., and Franke, S.: Terdiurnal wave signatures in the upper mesospheric
587 temperature and their association with the wind fields at low latitudes (20◦N), J. Geophys.
588 Res., 110, D09S06, doi: 10.1029/2004JD004564, 2005.

589 Taori, A., Jayaraman, A., Kamalakar, V.: Imaging of mesosphere–thermosphere airglow
590 emissions over Gadanki (13.51N, 79.21E)-first results, J. Atmos. Sol. Terr. Phys. 93, 21–28,
591 http://dx.doi.org/10.1016/j.jastp.2012.11.007, 2013.

592 Tarasick, D. W., and Shepherd, G. G.: Effects of gravity waves on complex airglow chemistries:
593 1. $O_2(b^1\sum^+_g)$ emission, J. Geophys. Res., 97, 3185–3193, 1992a.

594 Tarasick, D. W., and Shepherd, G. G.: Effects of gravity waves on complex airglow chemistries:
595 2. OH emission, J. Geophys. Res., 97, 3195–3208, 1992b.

596 Vargas, F., Swenson, G., Liu, A., and Gobbi, D.: $O(^1S)$, OH, and O_2(b) airglow layer
597 perturbations due to AGWs and their implied effects on the atmosphere, J. Geophys. Res, 112,
598 D14102, doi:10.1029/2006JD007642, 2007.

599 Viereck, R. A., and Deehr, C. S.: On the interaction between gravity waves and the OH Meinel
600 (6-2) and O2Atmospheric (0-1) bands in the polar night airglow, J. Geophys. Res., 94, 5397–
601 5404, 1989.

602 Walterscheid, R. L., and Schubert, G.: Dynamical-chemical model of fluctuations in the OH
603 airglow driven by migrating tides, stationary tides, and planetary waves, J. Geophys. Res.,
604 100, 17,443–17,449, 1995.

605 Walterscheid, R. L., and Hickey, M. P.: One-gas models with height-dependent mean molecular
606 weight: Effects on gravity wave propagation, J. Geophys. Res., 106, 28,831-28,839, 2001.

607 Walterscheid, R. L., Schubert, G., and Hickey, M. P.: A Comparison of Theories for Gravity
608 Wave Induced Fluctuations in Airglow Emissions, J. Geophys. Res., 99, 3935, 1994.

609 Walterscheid, R. L., Schubert, G., and Hickey, M. P.: Comparison of theories for gravity wave
610 fluctuations in airglow emissions, J. Geophys. Res., 99, 3935–3944, 1994.

611 Walterscheid, R. L., Schubert, G., and Straus, J. M.: A dynamical chemical model of wave-
612 driven fluctuations in the OH nightglow, J. Geophys. Res., 92, 1241 – 1254, 1987.

613

614

615

Figure captions:

Figure 1. Nocturnal variability in the mesospheric OH emissions on 26-27 January 2011. The upper panels represent the mean deviations in (a) intensity and (b) temperature data. Bottom panels represent (c) intensity and (d) temperature residuals. Solid line curves in each plot show the result of simple best-fit cosine model.

Figure 2 (a) Distribution of Krassovsky parameter 'η', reported by investigators (list not exhaustive). The x -axis shows the wave periodicity and the y-axis is for amplitude of Krassovsky parameters (η) The legends in the figure are as following: (1 (for 2010 year) & 2 (for 2011 year)- present study ; 3,Schubert et al. 500 km; 4, Schubert et al. 1000 km; 5, Tarasick and Shepherd 500 km; 6,Tarasick and Shepherd 1000 km; 7, Takahashi et al. (1992); 8, Oznovich et al. (1995); 9, Drob et al. (1996); 10, Reisin and Scheer (1996); 11, Taylor et al. (2001); 12, Guharay et al (2008); 13, Walterscheid and Schubert (1995); 14, Lopez-Gonzalez et al. (2005); 15, Oznovich et al. (1997)); 16, Viereck and Deehr (1989).

Figure 2 (a1) Observed values of η versus wave period over Kolhapur alone.

Figure 2 (b) Distribution of phase values of Krassovsky parameter 'Φ', reported by investigators (list not exhaustive) (1 (for year 2010) & 2 (for year 2011)- present study; 3,Schubert et al. 500 km; 4, Schubert et al. 1000 km; 5, Tarasick and Shepherd 500 km; 6, Tarasick and Shepherd 1000 km; 7,Viereck and Deehr (1989); 8, Oznovich et al. (1995); 9, Drob et al. (1996); 10, Reisin and Scheer (1996); 11, Taylor et al. (2001); 12, Guharay et al.(2008); 13, Walterscheid and Schubert (1995); 14, Lopez-Gonzalez et al. (2005); 15, Oznovich et al. (1997); 16,Viereck and Deehr (1989);).

Figure 2 (b1) Observed values of Φ verses wave period over Kolhapur alone.

Figure 2(c) Deduced vertical wavelength (VW) for both the short and long period wave as function of wave periodicity. Also shown comparison with values obtained by other investigators.

Figure 3(a) Comparison with η calculated by observation of both year and Full wave model simulation with their respective wave period. Pink and olive lower half filled square shows the 2010 and 2011 year η observations (1 and 2 present study η: 3,FWM simulation of η for 50 m/s horizontal phase velocity; 4, FWM simulation of η for 100 m/s horizontal phase velocity; 5, FWM simulation of η for 150 m/s horizontal phase velociy).

Figure 3(b) Simillar to figure 3(a) but for phase values for both the short and long period wave.

Figure 3(c) Simillar to figure 3(a) but for deduced vertical wavelength (VW).

Figure 4. The monthly (February, March and April) mean OH emission rate profiles from SABER for the year 2010 (solid lines) and 2011 (dashed lines).

Table 1. Comparisons of deduced wave parameters in 2010,2011 years with MEI index and OH altitudes. The observed quantities are mean for their representative wave periods. (JFM-January, February and March months like this)

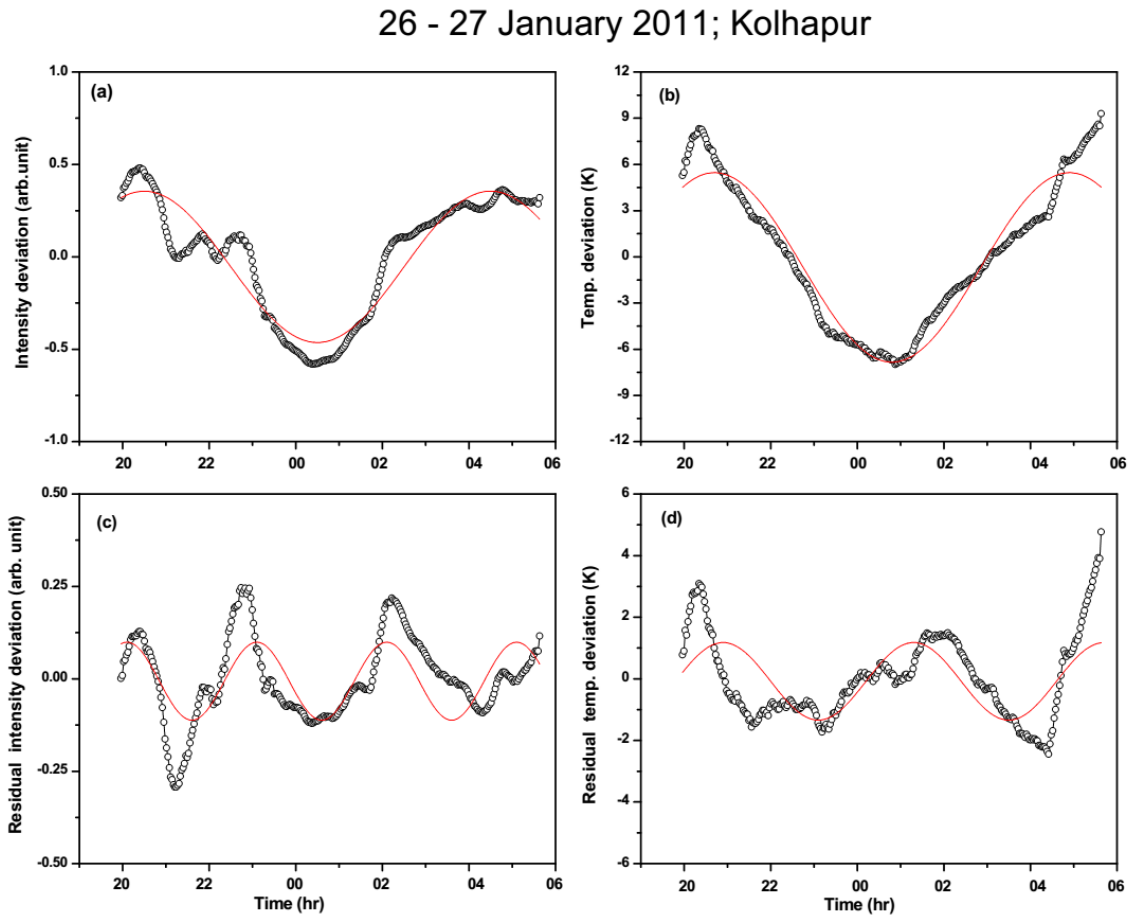
26 - 27 January 2011; Kolhapur
(a)
(b)
(c)
(d)
Intensity deviation (arb.unit)
Temp. deviation (K)
Residual intensity deviation (arb. unit)
Residual temp. deviation (K)
Time (hr)
Time (hr)
20
22
00
02
04
06

Figure 1.

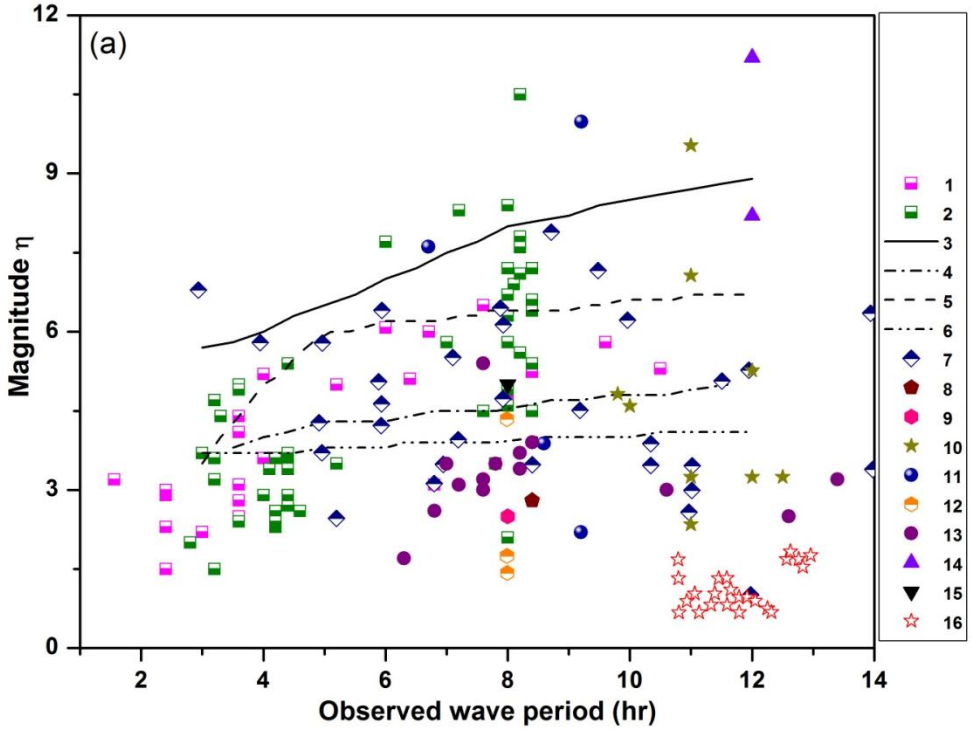

659

660 Figure 2(a)

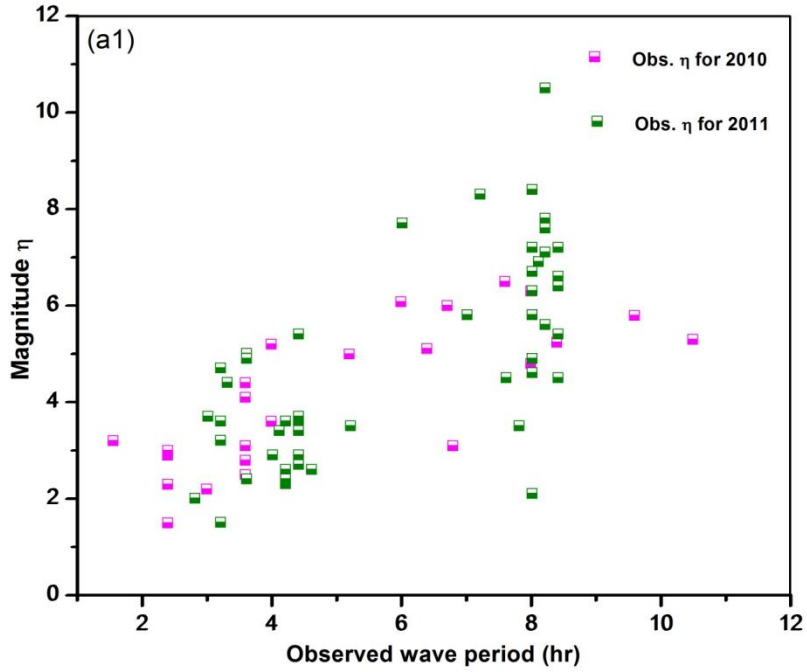

661

662 Figure 2(a1)

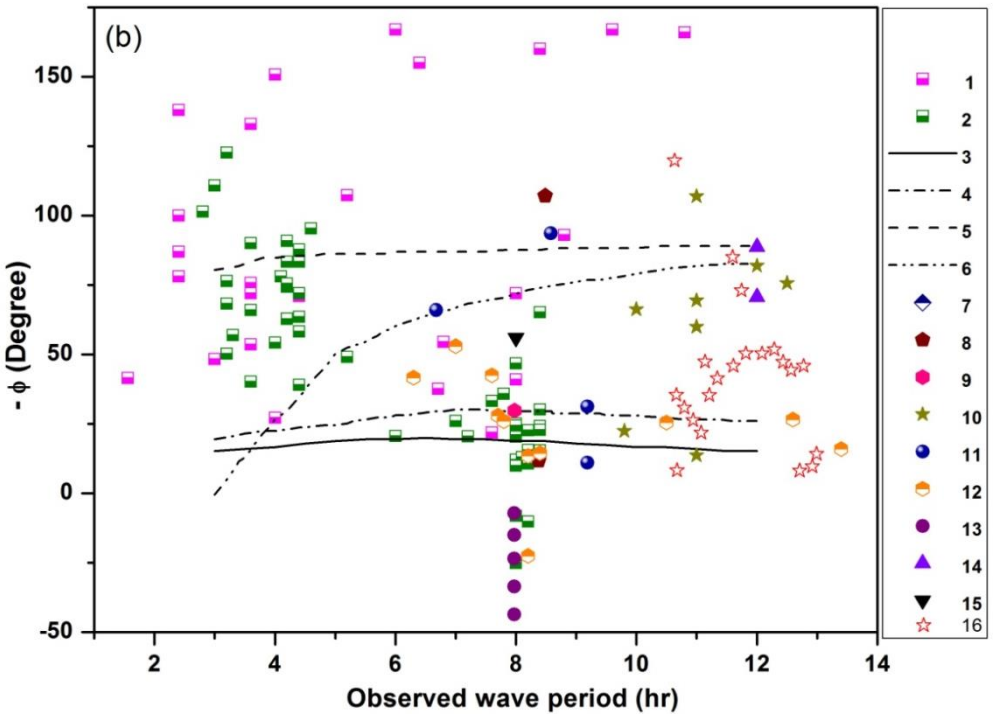

664 Figure 2(b)

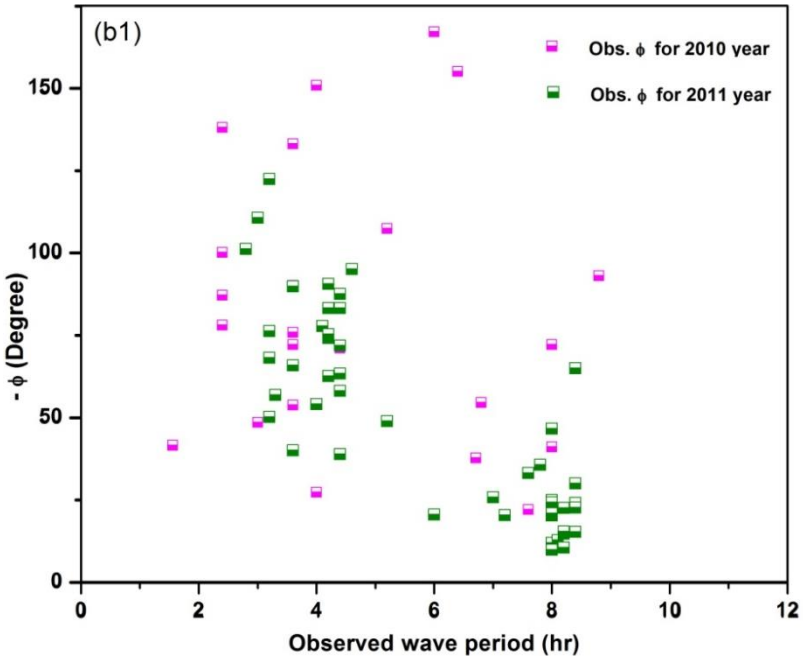

666

667 Figure 2(b1)

668

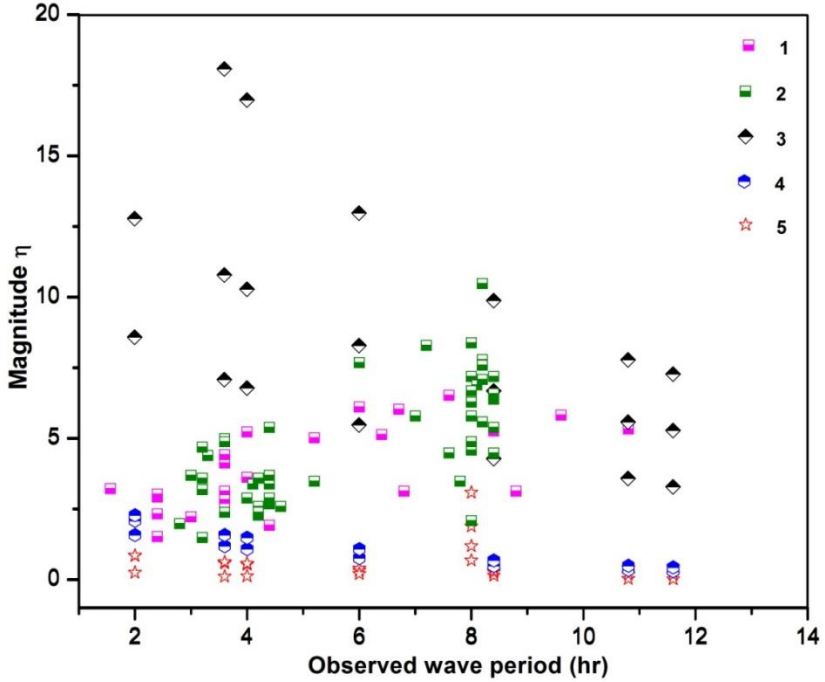

675 Figure 2(c)

676

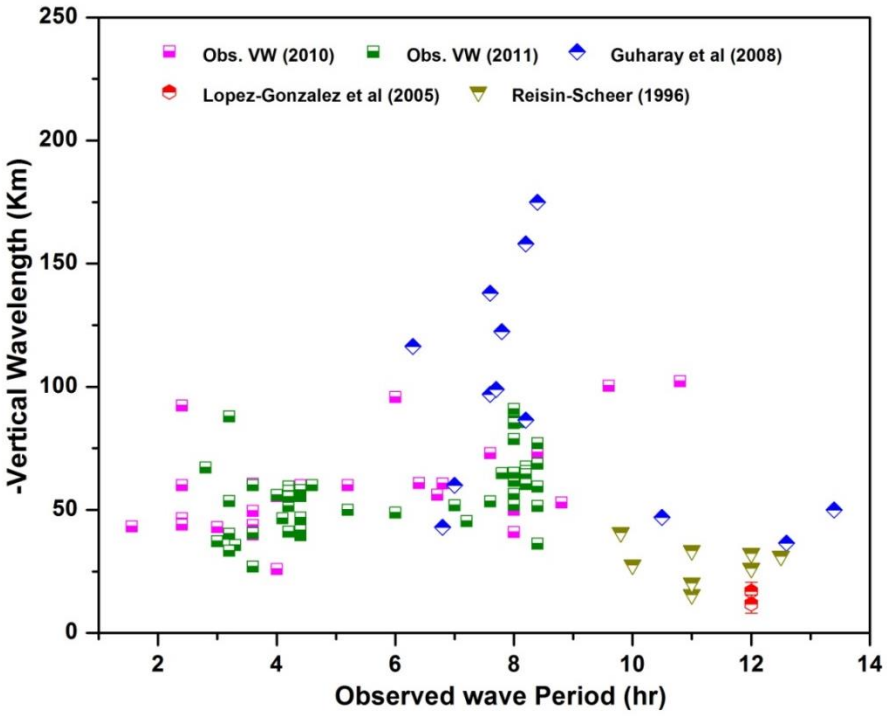

677

678 Figure (3a)

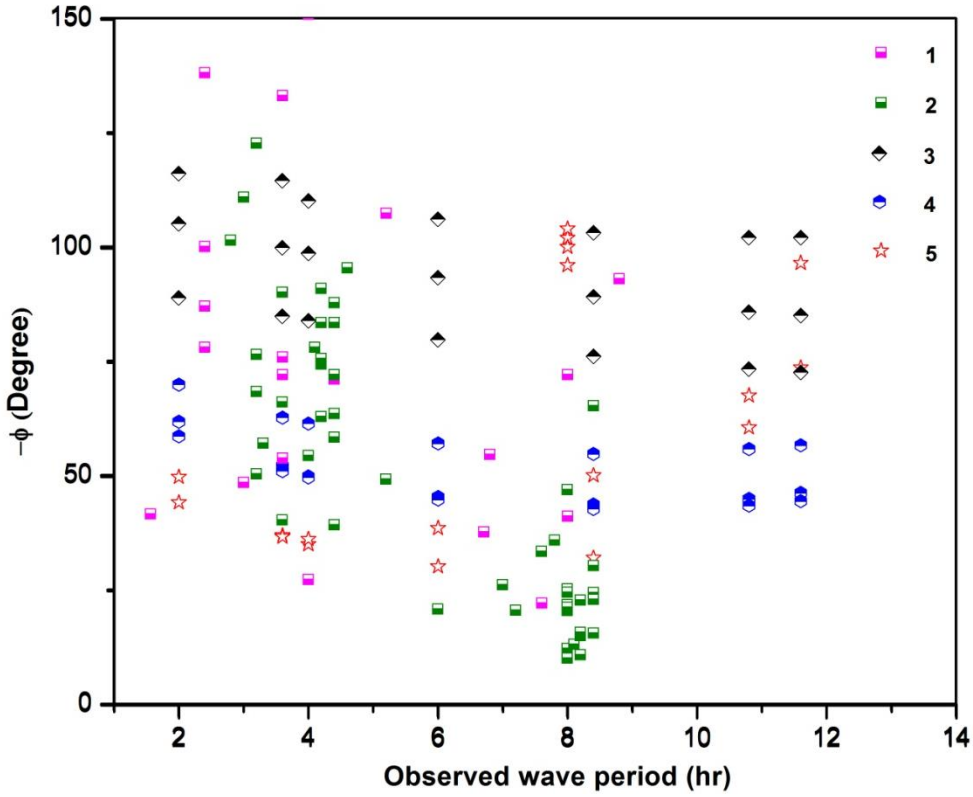

679

680 Figure 3(b)

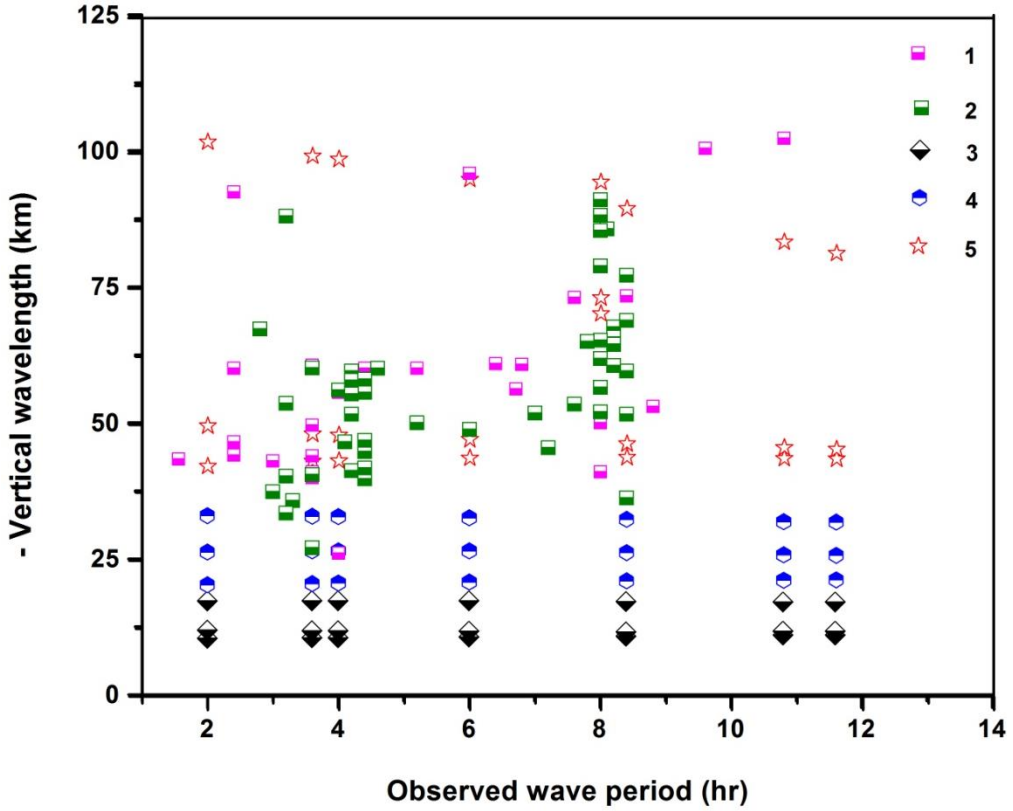

681

682 Figure 3 (c)

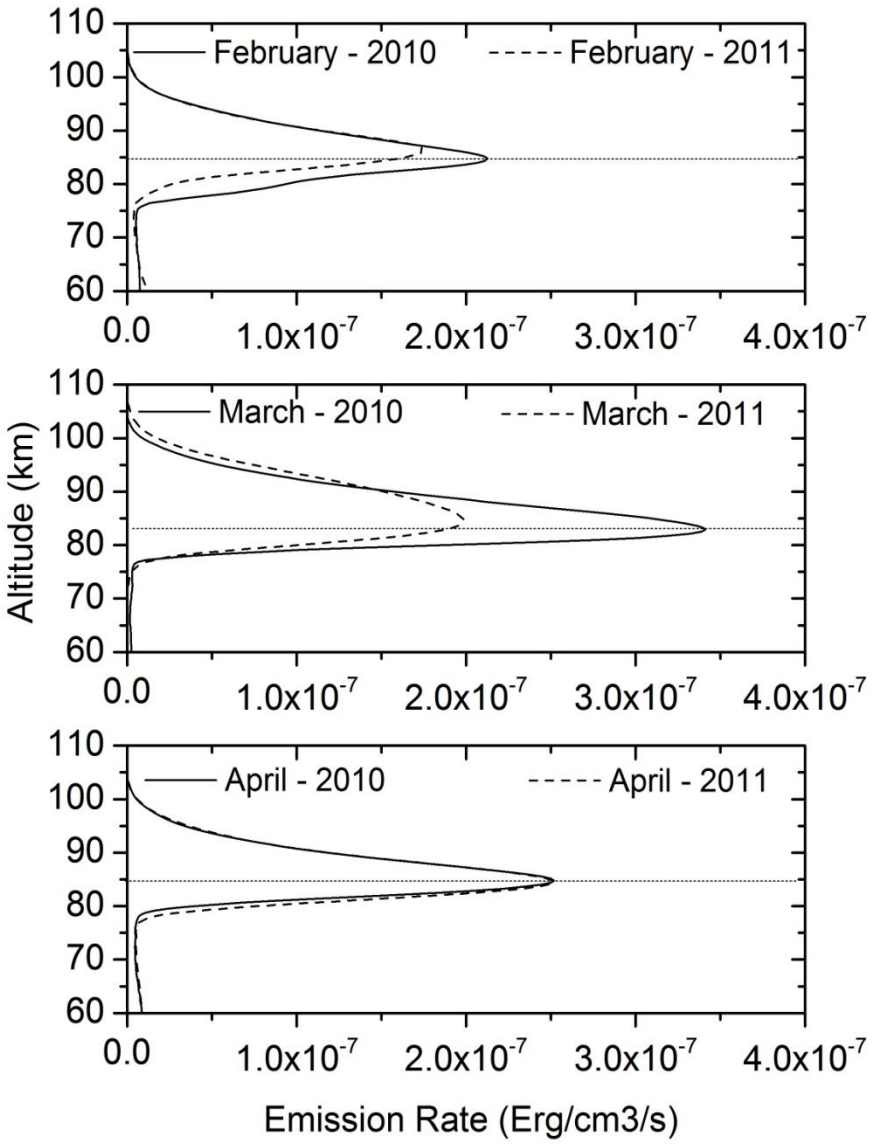

683

684 Figure 4.

685

686

687

688

689

690 Table 1.

Year	**Mean η** (± Errors)		**Mean (-Φ) (Deg.)**		**Mean (-VW) (km)**		**OH altitude (km)**	**MEI index**				
	Long wave period	Short wave period	Long wave period	Short wave period	Long wave period	Short wave period		JFM	FMA	MAM	SON	OND
2010	4.4 ± 1	2.3 ±0.9	90.6±40	70.4± 45	60.2 ± 20	42.8 ± 15	82 km to 85.1 km during February – April	1.1	0.8	0.5	-1.4	-1.3
2011	5.7 ± 1.7	2.7 ±0.6	33.8±40	64.4± 40	77.6 ± 40	59.2 ± 30	85.1 km to 86 km during February – April	-1.1	-0.8	-0.6	-0.9	-0.9

691

692